Journal of the Serbian Chemical Society

JSCS-info@shd.org.rs • www.shd.org.rs/JSCS

J. Serb. Chem. Soc. 75 (12) 1671–1683 (2010)
JSCS–4087

UDC 547.979.733:539.194:532.14
Original scientific paper

Consistent force field for metalloporphyrins

LJUBICA ANDJELKOVIĆ[1], SONJA GRUBIŠIĆ[1#], IVANA DJORDJEVIĆ[1], MATIJA ZLATAR[1], SVETOZAR NIKETIĆ[1#] and MAJA GRUDEN-PAVLOVIĆ[2*#]

[1]*Center for Chemistry, Institute of Chemistry, Technology and Metallurgy, University of Belgrade, Njegoševa 12, 11001 Belgrade and* [2]*Faculty of Chemistry, University of Belgrade, Studentski Trg 12–16, 11001 Belgrade, Serbia*

(Received 1 July 2010)

Abstract: Molecular mechanics (MM) calculations to analyze the puckering of metalloporphyrins isolated and adsorbed on a graphite layer (0001) as a function of metal ion size and the peripheral substitution are presented. The Consistent Force Field (CFF) program was used with new parameters for metalloporphyrins, which included an out-of-plane bending function. Normal-coordinate structural decomposition (NSD) analysis was performed on the equilibrium structures obtained by the MM calculations. The conformers were also stereochemically characterized and compared with available experimental data and with conformers obtained in a previous MM study.

Keywords: porphyrins; graphite (0001) surface; molecular mechanics; non-planar conformations.

INTRODUCTION

Metalloporphyrins not only have important biological functions, but they can also be applied in many different industries. Among other applications, they were successfully employed for olefin epoxidation and alkane hydroxylation reactions as remarkably effective catalysts.[1]

It is well known that the porphyrins macrocycle displays a range of distorted non-planar shapes.[2–5] The non-planarity of the porphyrin core has profound consequences on the spectral, electrochemical and other properties of porphyrins, including functionality.[6] It was revealed that factors which induce non-planarity can be divided into at least four categories: peripheral substitution, the central metal, axial ligation and the environment of the porphyrin.[7] Previous studies showed that the type and degree of non-planar deformation can be controlled by the peripheral substitution pattern, the steric bulkiness of substituents and the size

* Corresponding author. E-mail: gmaja@chem.bg.ac.rs
# Serbian Chemical Society member.
doi: 10.2298/JSC100701095A

of central metal ion of the macrocycle.[8,9] Furthermore, it was also shown that adsorption of metalloporphyrins on a graphite layer influences conformational changes of the porphyrin core.[10]

Theoretically, the complete set of normal coordinates for a macrocycle forms a basis for describing any distortion of a porphyrin core. For a porphyrin of D_{4h} symmetry, the distortion can be divided into in-plane and out-of-plane deformations. Only a few of the lowest frequency modes are required to adequately describe the out-of-plane distortions.[11] These are: ruffing (*ruf*, B_{1u}), saddling (*sad*, B_{2u}), doming (*dom*, A_{2u}), two wavings (*wav*$_x$, *wav*$_y$, E_g) and propellering (*pro*, A_{1u}), which are shown in Fig. 1. Many experimental techniques have been used for distinguishing the magnitude of non-planar distortion, although distinguishing the different types of distortion (*ruf*, *sad*, *dom*, *wav* and *pro*) has proved to be more challenging.[12] Molecular modeling, developed for the investigation of non-planar porphyrins, provides information about the energetics of non-planar distortions, as well as, additional structural information.[13] In this work, molecular mechanics (MM) calculations were used to study the effects of peripheral substitution, the nature of the central metal atom and the influence of the graphite (0001) surface on the non-planar distortions of metalloporphyrins. Although, some of the porphyrin molecules mentioned in this paper have already been analyzed, recently force field was supplemented with a new function and hence, all parameters were reoptimized in order to improve their reliability, in other words, to improve their accuracy in producing a physically meaningful potential energy surface.

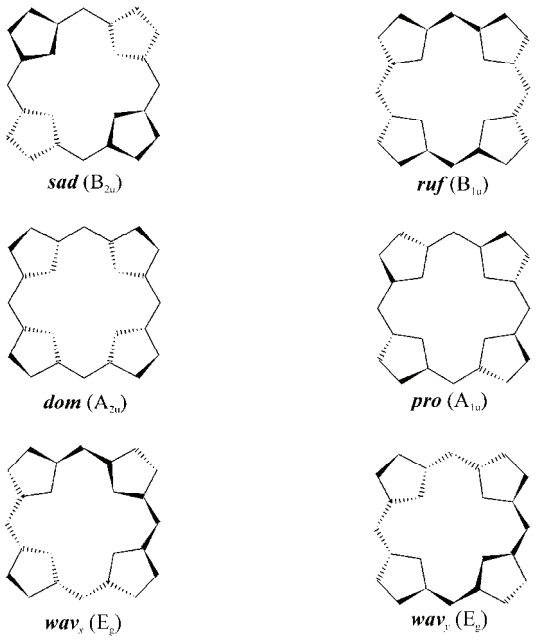

Fig. 1. Non-planar porphyrin-core conformations. Bold and dashed lines represent core fragments lying below and above the mean plane, respectively.

COMPUTATIONAL DETAILS

Molecular mechanics calculations were performed with the 2007/PC version of the Consistent force field (CFF) conformational program.[14] Conformational energy was defined in the usual way as given in Eq. (1):

$$E_{\text{tot}} = \sum E_{\text{b}} + \sum E_{\theta} + \sum E_{\varphi} + \sum E_{\text{nb}}^{(\text{intramol.+intermol.})} + \sum E_{\text{e}}^{(\text{intramol.+intermol.})} + \sum E_{\text{oop}} \qquad (1)$$

where the terms on the right-hand side represent bond-stretching, angle-bending, torsional, non-bonded, Coulomb, and out-of-plane bending contributions, respectively. Bond-stretching and angle-bending contributions were treated with simple harmonic functions (Eq. (2)). Torsional contributions were represented as Fourier series that accounts for all four torsions involving a double bond, or nine torsions involving a single bond.

Non-bonded intramolecular van der Waals interactions were modeled using the Lennard--Jones "12-6" potential function with parameters which were chosen by extrapolation based on the available parameter sets, imposing their consistency with the original force field.[15,16]

Non-bonded intramolecular electrostatic contributions were modeled with the Coulomb function.

Point charges were obtained from *ab-initio* calculations (Gaussian 98).[17]

Out-of-plane bending was defined by using the height of the pyramid formed by the four atoms (Fig. 2, Eq. (2)). This function was added to the CFF conformational program where *h*oop is the perpendicular distance of atom *i* from the plane defined by atoms *jkl*, and *k*oop is the force constant.[18]

$$E_{\text{tot}} = \sum_{r}\frac{1}{2}k_r(r-r^0)^2 + \sum_{\theta}\frac{1}{2}k_\theta(\theta-\theta^0)^2 + \sum_{\varphi}\frac{1}{2}(1+\cos n\varphi) + \sum_{ij}\left[\frac{2}{3}\varepsilon\left(\frac{r^*}{r}\right)^{12} - \varepsilon\left(\frac{r^*}{r}\right)^{6}\right] + \\ + \sum_{ij}\frac{q_i q_j}{\varepsilon_{ij} r_{ij}} + \sum k_{\text{oop}} h_{\text{oop}}^2 + \sum_i \sum_j \frac{1}{r_{ij}^3} q_i \left(e^T \theta_j e\right) \qquad (2)$$

Intermolecular van der Waals interactions between the porphyrin macrocycle and the graphite C atoms were treated with the Lennard-Jones "12-6" type function, with the same parameters as for intramolecular potential.

Modeling of the graphite layer was described in a previous paper.[10]

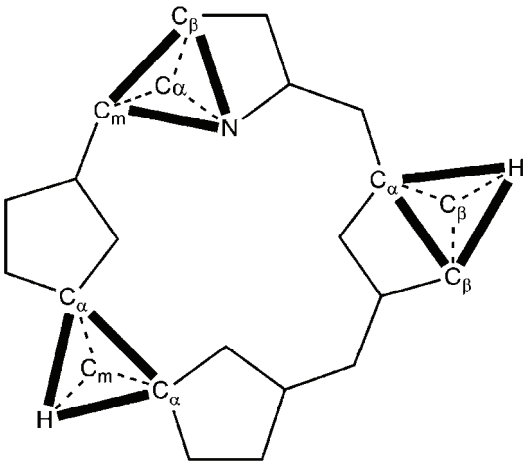

Fig. 2. Out-of-plane bending functions: $NC_mC_\beta C_\alpha$, $C_\alpha HC_\beta C_\beta$ and $C_\alpha HC_\alpha C_m$. Atom types used in defining the force field parameters for the molecular mechanics calculation.

Intermolecular electrostatic interactions were treated as monopole–quadrupole interactions between point charges located on the atomic positions of all metalloporphyrin atoms and uniaxial quadrupoles defined on each C atom of the graphite layer:

$$E^{(e,Q)} = \sum_i \sum_j \frac{1}{r_{ij}^3} q_i \left(e^T \theta_j e \right) \quad (3)$$

where q_i is the point charge on the *i*-th porphyrin atom; r_{ij} is the interatomic distance; e is the unit vector along r_{ij}; θ_j is the quadrupole moment tensor of the j-th C atom on the graphite layer (Eq. (3)).[10]

Non-bonded cut-off was treated with a cubic spline switching function with the spline-on distance of 7 Å and the spline width of 2 Å.

Geometry optimizations were realized using combinations of the steepest-descent, Davidon–Fletcher–Powell and Newton–Raphson methods.[14] Geometry optimizations were performed to the energy rms gradient of $< 10^{-6}$ kJ mol^{-1} Å^{-1}.

For each of the equilibrium structures obtained by the energy minimization procedure, normal-coordinate structural decomposition (NSD) analysis was performed using the software available at http://jasheln.unm.edu/. The NSD method provides a unique way for characterizing the distortions of the macrocycle and gives detailed analysis of the type of deformations present in the calculated porphyrin structures.

Force field parametrization

In this work, new function which describes out-of-plane bending interaction was added in the CFF conformational program for the first time and hence all the force field parameters on the available X-ray structures of Ni(II)porphyrin, Ni(II)mono-*tert*-butylporphyrin, Ni(II)di--*tert*-butylporphyrin, Ni(II)tetraphenylporphyrin and Ni(II)octaethyl-tetraphenylporphyrin were reoptimized by adjusting the appropriate parameters on a trial-and-error basis until the RMSD values between the calculated and crystallographically observed bond lengths and valence angels were ≤ 0.03 Å and $\leq 3°$, respectively.

The force field was parametrized based the four different types of carbon atoms (α and β pyrrole carbons, *meso* carbon of the porphyrin ring, aromatic carbon of the phenyl substituents and sp^3-hybridized C atom of the alkyl substituents), one type of hydrogen and of nitrogen, central metal atoms and the halogen substituents (chlorine and bromine).

The aim of involving the out-of-plane bending function was to assure persistency of planarity of selected fragments of metalloporphyrins in the optimized structures, as is indicated in Fig. 2. In earlier works, higher values of the torsional parameters were used in order to keep planarity of selected fragments in the porphyrin molecules, giving better agreement with the X-ray data. Hence, there was a need to introduce a new function in the CFF conformational program so that the torsional parameters could approach more realistic lower values.

The conformers obtained by MM calculations were stereochemically characterized, compared with available X-ray crystal structures, analyzed by the NSD method and also compared to the results obtained in a previous MM study without the out-of-plane bending function. Comparison of selected structural data for the molecules used in parametrization are given in Table I. These results indicate better agreement between calculated and X-ray structures, in comparison with previous results, establishing the reliability of the present force field, but did not affect any of previous conclusions.

A list of all force field parameters is given in Table S-I in the Supplementary material.

TABLE I. Selected average bond lengths (Å), valence and torsion angles (°) for the equilibrium metalloporphyrins structures and for available crystal structures. Missing values are not reported (–) in the cited sources

Method	Ni–N	C_β–C_β	C_α–C_m	N–C_α	N–Ni–N	C_α–N–C_α	N–C_α–C_β–C_β	N–C_α–C_m–C_α
NiP								
X-Ray[a]	1.951	1.347	1.371	1.379	179.3	104.3	0.3	0.8
MM[b]	1.912	1.336	1.366	1.377	179.9	103.8	0.02	0.0
MM	1.945	1.340	1.375	1.375	180.0	105.5	0.9	1.2
NiMtBuP								
X-Ray[c]	1.901	1.342	1.380	1.380	178.9	106.3	3.0	11.1
MM[d]	1.917	1.338	1.372	1.377	177.3	105.2	4.5	14.3
MM	1.944	1.338	1.377	1.376	177.3	103.5	0.86	1.19
NiDtBuP								
X-Ray[e] (αα)	1.900	1.353	1.394	1.383	177.0	106.2	2.9	14.8
MM[d]αα	1.900	1.341	1.379	1.373	177.6	106.0	5.4	25.1
MMαα	1.934	1.338	1.380	1.376	176.8	106.3	8.8	23.6
MM[d]αβ	1.910	1.337	1.378	1.377	179.9	103.9	6.1	19.1
MMαβ	1.934	1.340	1.379	1.375	177.2	103.3	18.26	21.02
NiTPP								
X-Ray[f]	1.931	1.340	1.383	1.377	180.0	104.9	2.6	9.6
MM[b]	1.930	1.337	1.370	1.377	180.0	104.9	1.4	11.8
MM	1.964	1.334	1.376	1.378	176.2	106.3	4.2	8.7
NiOEtTPP								
X-ray[g]	1.906	1.365	1.395	1.381	90.6	105.9	–	–
MM[h]	1.875	1.341	1.375	1.375	90.4	106.3	–	–
MM	1.924	1.347	1.348	1.376	90.6	108.2	–	–

[a]W. Jentzen, I. Turowska-Tyrk, W. R. Scheidt, J. A. Schelnutt, *Inorg. Chem.* **35** (1996) 3559; [b]M. Gruden-Pavlović, S. Grubišić, S. R. Niketić, *J. Inorg. Biochem.* **98** (2004) 1293; [c]X.-Z. Song, W. Jentzen, L. Jaquinod, R. G. Khoury, C. J. Medforth, S.-L. Jia, J.-G. Ma, K. M. Smith, J. A. Shelnutt, *Inorg. Chem.* **37** (1998) 2117; [d]M. Gruden, S. Grubišić, A. G. Coutsolelos, S. R. Niketić, *J. Mol. Struct.* **595** (2001) 209; [e]X. Z. Song, W. Jentzen, S. L. Jia, L. Jaquinod, D. J. Nurco, C. J. Medforth, K. M. Smith, J. A. Shelnutt, *J. Am. Chem. Soc.* **118** (1996) 12975; [f]A. L. MacLean, G. J. Foran, B. J. Kennedy, P. Turner, T. W. Hambley *Austral. J. Chem.* **49** (1996) 1273; [g]K. M. Barkigia, M. W. Renner, L. R. Furenlid, C. J. Medforth, K. M. Smith, J. Fajer, J. *Am. Chem. Soc.* 115 (1993) 3627; [h]Unpublished work

RESULTS AND DISCUSSION

The effects of peripheral substitution of various substituents, coordination of central metal ions of different radii and adsorption of molecules on the graphite layer (0001) on the conformations of porphyrin macrocycle of octa- and tetrahalogenated (chloro and bromo) tetraphenylporphyrin (TPP) derivates with Ni(II) an Tb(III) metal ions were studied. Ni(II) metal ion and Tb(III) metal ion were chosen to represent central metal atoms with a relatively small and large radius, respectively. As in a previous study, the initial structures for tetrahalogeno TPP were chosen based on the most symmetrical substitution pattern of the halogens and comprised: 2,8,12,18-tetrahalogeno-TPP (trans-trans, or tt)

isomer; 2,3,12,13-tetrahalogeno-TPP (cis-trans, or ct); 2,7,12,17-tetrahalogeno-TPP (windmill, or wm) isomer.

All the stable conformers for the series of porphyrins were obtained by energy minimization starting from five (plan, sad, ruf, dom, wav) initial structures. Furthermore, for the porphyrin macrocycles adsorbed on the graphite surface, two different positions of the metal (one with the metal atom directly above a given graphite carbon atom and the other with the metal located above the hole of the graphite hexagon) and various intermolecular distances (3–8 Å, in steps of 0.5 Å) were considered.

It is noteworthy that the geometrical optimization resulted in one unique equilibrium conformation for all the investigated porphyrin structures, regardless of the initial structures that were started with.

Isolated structures

The structural parameters for the energy-minimized conformers, as well as a comparison with the available crystal structures, are given in Table II; the

TABLE II. Selected average bond lengths (Å), valence and torsion angles (°) for the equilibrium, isolated metalloporphyrins structures and for crystal structures

Method	M–N	N–C_α	C_β–C_β	C_α–C_m	X[a]–C_β	N–M–N	C_α–N–C_α
			Ni(II)Br_xTPP				
X-Ray[b]	1.900	1.380	1.340	1.380	1.870	168.5	106.6
Br_8	1.924	1.374	1.349	1.384	1.911	166.5	108.7
ct-Br_4	1.951	1.337	1.334	1.379	1.903	90.8	105.3
tt-Br_4	1.944	1.376	1.340	1.380	1.898	90.4	106.7
wm-Br_4	1.948	1.376	1.339	1.379	1.896	90.5	107.6
			Ni(II)Cl_xTPP				
X-Ray[c]	1.904	1.384	1.348	1.394	1.705	90.3	107.3
Cl_8	1.932	1.376	1.345	1.383	1.737	90.7	108.3
ct-Cl_4	1.953	1.378	1.338	1.378	1.733	90.6	105.8
tt-Cl_4	1.947	1.376	1.338	1.379	1.730	90.4	107.3
wm-Cl_4	1.950	1.377	1.338	1.379	1.730	90.4	107.5
			Tb(III)Br_xTPP				
Br_8	2.311	1.377	1.342	1.386	1.899	86.1	105.2
ct-Br_4	2.309	1.378	1.340	1.386	1.902	86.7	105.9
tt-Br_4	2.307	1.376	1.341	1.387	1.901	85.6	106.6
wm-Br_4	2.308	1.377	1.340	1.386	1.896	86.1	107.3
			Tb(III)Cl_xTPP				
Cl_8	2.304	1.376	1.346	1.388	1.738	85.1	107.1
ct-Cl_4	2.308	1.376	1.342	1.386	1.733	85.3	108.4
tt-Cl_4	2.308	1.377	1.340	1.387	1.732	85.7	106.8
wm-Cl_4	2.308	1.377	1.340	1.386	1.729	86.1	107.3

[a]Br,Cl; [b]X-Ray data of Ni(II)Br_8TPP, L. M. Henling, W. P. Schaefer, J. A. Hodge, M. E. Hughes, H. B. Gray, *Acta Cryst. C* **49** (1993) 1743; [c]X-Ray data of Ni(II)Cl_8TPP Ni, G. A. Spyroulias, A. P. Despotopoulos, C .P. Raptopoulou, A. Terzis, D. de Montauzon, R. Poilblance, A. G. Coutsolelos, *Org. Chem.* **41** (2002) 2648

calculated energy distributions are listed in Table III and the results of the NSD analysis for all the optimized molecules are presented in Table IV.

TABLE III. Energy contributions (in kcal mol^{-1}) for the isolated, equilibrium TPP conformations

Species	E_{tot}	E_{bond}	E_{angle}	$E_{torsion}$	E_{oop}	E_{vdw}	E_c	E_{nb}
Ni(II)Br$_x$TPP								
Br_8	55.28	4.72	15.55	18.83	1.39	26.53	–11.74	14.79
ct-Br_4	35.83	1.97	9.99	16.14	1.32	17.95	–11.55	6.40
tt-Br_4	35.51	1.90	8.56	16.71	1.42	18.68	–11.76	6.93
wm-Br_4	33.81	1.80	8.90	14.83	1.51	18.48	–11.72	6.76
Ni(II)Cl$_x$TPP								
Cl_8	54.09	3.05	12.36	17.83	1.61	23.53	–4.29	19.24
ct-Cl_4	36.32	1.68	8.64	14.90	1.25	18.59	–8.73	9.86
tt-Cl_4	34.64	1.70	8.11	15.98	1.37	19.19	–11.70	7.48
wm-Cl_4	32.91	1.61	8.36	14.51	1.49	18.84	–11.90	6.95
Tb(III)Br$_x$TPP								
Br_8	75.17	5.20	22.30	38.21	4.55	13.83	–8.92	4.91
ct-Br_4	56.07	4.97	20.1	21.97	2.06	15.73	–8.75	6.98
tt-Br_4	61.21	5.39	24.18	18.59	2.61	19.25	–8.79	10.45
wm-Br_4	57.48	4.92	23.01	19.08	2.52	16.74	–8.78	7.96
Tb(III)Cl$_x$TPP								
Cl_8	84.93	6.83	31.06	19.59	2.94	25.31	–0.81	24.50
ct-Cl_4	64.69	5.30	25.7	16.10	2.51	20.25	–5.16	15.09
tt-Cl_4	60.08	5.11	23.56	17.46	2.49	19.7	–8.24	11.46
wm-Cl_4	56.7	4.79	22.59	17.98	2.38	17.33	–8.36	8.97

The NSD analysis revealed that the structure of Ni(II)Br8TPP is pure saddle and it shows the largest deviation from planarity (Table IV). The ct--isomer of Ni(II)Br4TPP is a mixture of sad and dom non-planar deformations, the tt-isomer is almost pure saddle with a minor contribution of the pro mode, while the optimized structure of the wm-isomer indicated that it consisted of sad and a small amount of ruf deformations. For the tetrabromo-TPP–Ni(II) complexes, the wm-isomer is the most stable one (Table III).

The Ni(II)Cl8TPP complex is also highly puckered, and the NSD analysis indicated an almost pure saddled macrocycle. All three isomers of Ni(II)Cl4TPP possess sad as the dominant deformation, with contributions of dom, pro and ruf distortions for ct-, tt- and wm-isomer, respectively.

For the octa- and tetrabromo substituted structures with the very large Tb(III) ion, the dom deformation was present in all structures as was expected (Table IV). The NSD analysis revealed that the structure of the Tb(III)Br8TPP complex is a mixture of dom, sad, ruf and pro deformations. In the case of the ct-isomer of Tb(III)Br4TPP, the metal ion favors dom distortion, and saddling is favored by the substituents. An almost equal ratio of sad and dom deformations

was found in the tt-isomer and in the case of wm-isomer, the sad distortion dominates. The ct-isomer is the most stable one, but the difference between total energy of the ct- and wm-isomer is not so significant (Table III).

TABLE IV. Results of the normal-coordinate structural decomposition (NSD) analysis for the equilibrium, isolated TPP conformations. D_{oop} is the total out-of-plane distortion (in Å)

Species	D_{oop}	*sad*	*ruf*	*dom*	*wav(x)*	*wav(y)*	*pro*
			Ni(II)Br$_x$TPP				
Br_8	3.7365	3.7365	0.0083	0.0057	0.0057	0.0084	0.0030
ct-Br_4	2.5544	2.3495	0.0171	1.0021	0.0153	0.0144	1.0100
tt-Br_4	2.4576	2.4426	0.0058	0.0105	0.0091	0.0143	0.2704
wm-Br_4	2.3550	2.3236	0.3825	0.0164	0.0080	0.0162	0.0028
			Ni(II)Cl$_x$TPP				
Cl_8	3.3397	3.3397	0.0065	0.0057	0.0059	0.0080	0.0037
ct-Cl_4	2.2829	2.1277	0.0141	0.8270	0.0115	0.0121	0.0079
tt-Cl_4	2.3360	2.3253	0.0053	0.0102	0.0084	0.0138	0.2219
wm-Cl_4	2.1913	2.1475	0.4354	0.0147	0.0074	0.0151	0.0022
			Tb(III)Br$_x$TPP				
Br_8	2.2838	1.4672	0.5068	1.6167	0.0446	0.0322	0.4353
ct-Br_4	1.8914	0.7306	0.0156	1.7440	0.0311	0.0225	0.0206
tt-Br_4	1.9571	1.4579	0.0341	1.2637	0.0121	0.0027	0.3263
wm-Br_4	3.0589	2.7552	0.0416	1.3281	0.0139	0.0033	0.0088
			Tb(III)Cl$_x$TPP				
Cl_8	3.0589	2.7552	0.0416	1.3281	0.0139	0.0033	0.0088
ct-Cl_4	1.5314	0.9842	0.0115	1.1732	0.0087	0.0066	0.0053
tt-Cl_4	2.9150	2.1099	0.5525	1.1933	0.5995	1.3628	0.3152
wm-Cl_4	3.0589	2.7552	0.0416	1.3281	0.0139	0.0033	0.0088

In optimized structure of the Tb(III)Cl8TPP complex, sad and dom normal modes were observed (Table IV). The NSD analysis of the ct-isomer of Tb(III)Cl4TPP shows an almost equal ratio of dom and sad distortions. The shape of optimized conformation of the tt-isomer is a combination of the five most commonly observed distortions, with domination of the sad deformation mode. In the case of the wm-isomer, the ratio of the sad and dom deformations is almost the same as for the wm-isomer of Tb(III)Br4TPP. As in the case of the tetrachloro substituted TPP isomers, the wm isomer is the most stable (Table III).

Adsorbed structures

The structural parameters for the energy-minimized conformers are presented in Table V, the calculated energy distributions are listed in Table VI and the results of NSD analysis for all the investigated porphyrins adsorbed on a graphite layer are listed in Table VII.

TABLE V. Selected average bond lengths (Å), valence and torsion angles (°) for the equilibrium, adsorbed metalloporphyrins structures

Species	M–N	N–C_α	C_β–C_β	C_α–C_m	X[a]–C_β	N–M–N	C_α–N–C_α
			Ni(II)Br_xTPP				
Br_8	1.925	1.375	1.348	1.385	1.911	166.7	108.80
ct-Br_4	1.962	1.379	1.338	1.378	1.902	90.02	107.54
tt-Br_4	1.968	1.376	1.335	1.376	1.901	90.42	106.80
wm-Br_4	1.971	1.376	1.334	1.374	1.899	89.98	107.54
			Ni(II)Cl_xTPP				
Cl_8	1.945	1.378	1.341	1.384	1.739	90.6	108.60
ct-Cl_4	1.972	1.379	1.334	1.376	1.733	89.98	106.89
tt-Cl_4	1.965	1.376	1.334	1.374	1.735	90.51	106.82
wm-Cl_4	1.971	1.380	1.334	1.372	1.738	90.23	106.72
			Tb(III)Br_xTPP				
Br_8	2.300	1.377	1.344	1.392	1.899	86.5	108.9
ct-Br_4	2.303	1.376	1.340	1.392	1.901	86.8	109.7
tt-Br_4	2.303	1.375	1.339	1.388	1.902	86.2	109.8
wm-Br_4	2.302	1.378	1.340	1.388	1.899	86.3	109.7
			Tb(III)Cl_xTPP				
Cl_8	2.300	1.382	1.343	1.396	1.740	86.6	112.3
ct-Cl_4	2.303	1.379	1.343	1.389	1.737	85.9	109.6
tt-Cl_4	2.300	1.378	1.339	1.390	1.731	85.5	108.5
wm-Cl_4	2.302	1.379	1.342	1.388	1.740	85.6	109.2

[a]Br,Cl

NSD Pattern for structure of Ni(II)Br8TPP adsorbed on graphite surface is almost the same as for isolated molecule, because there is no significant intermolecular interaction (Table VI).

Distance of Ni(II) ion from graphite is approximately 6 Å. Large distance is explained by the presence of bulky groups and repulsive interaction between negative charges, hence the porphyrin macrocycle can not approach more closely to the graphite layer. Geometry optimization for three isomers of Ni(II)Br4TPP leads to parallel orientation of porphyrin macrocycle on graphite, where in all cases the metal ion is above the center of C–C bond. In comparison to the isolated structures, all three isomers adsorbed on a graphite layer are less puckered (Tables IV and VII). In the ct-isomer, an almost equal ratio of dom and sad distortions is observed (Table VII). The ruf and dom deformations dominate in the tt-isomer, with presence of the pro deformation mode, while the wm-isomer can be described with dom deformation and a small contribution of pro distortion.

After geometry optimization of the various initial conformations of the adsorbed molecule Ni(II)Cl8TPP, starting from the various distances from the graphite layer and different initial positions of metal ion in relation to graphite, the end result was a unique conformation, very similar to the isolated structure, with the sad mode as dominant, and with a small contribution of the dom dis-

tortion. Final position of the metal ion is exactly above center of the C–C bond of the graphite layer. The position of the metal ion in relation to the graphite layer of the three isomers of Ni(II)Cl4TPP is the same as in the case of the tetrabromo derivatives. NSD analysis revealed that all three isomers are more planar in comparison to the isolated structures (Tables IV and VII), which enhance the flattening π-stacking interactions. NSD analysis shows that in the ct-isomer, dom and sad deformations dominate. Almost all of the five most commonly observed distortions occur in the equilibrium conformation of the tt-isomer with domination of the ruf and dom modes. In the case of the wm-isomer, dom deformation is the dominant one, with a small contribution of pro distortion (Table VII).

TABLE VI. Energy contributions (in kcal mol^{-1}) for the equilibrium, adsorbed metalloporphyrins conformations

Species	E_{tot}	E_{bond}	E_{angle}	$E_{torsion}$	E_{oop}	E_{vdw}	E_c	E_{nb}	$E_{intervdw}$	E_{interc}	$E_{internb}$
Ni(II)Br$_x$TPP											
Br_8	46.33	4.61	16.15	18.36	1.26	27.11	–11.74	15.37	–5.83	–3.59	–9.42
ct-Br_4	–3.80	2.94	9.94	20.01	2.20	24.29	–11.11	13.17	–19.72	–32.33	–52.06
tt-Br_4	2.32	2.50	12.36	24.62	2.31	21.58	–11.28	10.29	–18.64	–31.12	–49.77
wm-Br_4	–5.40	2.22	11.83	19.67	2.09	20.92	–11.17	9.76	–20.41	–32.71	–53.11
Ni(II)Cl$_x$TPP											
Cl_8	23.48	3.65	16.54	17.44	1.40	32.53	–4.00	28.52	–29.81	–14.28	–44.09
ct-Cl_4	–16.41	2.58	10.35	19.16	2.12	23.16	–7.58	15.58	–20.07	–46.13	–66.21
tt-Cl_4	–15.74	2.26	12.08	25.1	2.13	27.76	–10.54	10.22	–18.25	–49.29	–67.55
wm-Cl_4	–17.69	2.09	13.24	22.42	1.88	20.81	–10.79	10.01	–19.7	–47.65	–67.35
Tb(III)Br$_x$TPP											
Br_8	12.66	6.2	24.28	35.49	3.03	13.81	–8.66	5.15	–29.81	–31.67	–61.48
ct-Br_4	16.84	10.35	29.84	19.09	1.48	20.51	–8.87	11.65	–19.55	–36.02	–55.57
tt-Br_4	16.04	7.59	25.64	21.26	2.02	14.68	–8.84	5.84	–17.68	–28.64	–46.32
wm-Br_4	12.28	9.23	30.76	17.01	1.28	17.5	–8.94	8.56	–19.88	–34.68	–54.56
Tb(III)Cl$_x$TPP											
Cl_8	36.32	8.81	36.07	23.57	2.89	35.05	–0.08	35.07	–19.71	–50.39	–70.09
ct-Cl_4	–4.48	5.32	30.33	22.05	3.15	19.01	–3.81	15.19	–17.88	–62.65	–80.54
tt-Cl_4	–4.84	5.00	32.45	25.5	2.94	17.29	–6.89	10.39	–17.24	–63.89	–81.14
wm-Cl_4	–7.54	4.82	31.75	24.44	2.77	16.17	–7.11	9.06	–18.37	–62.02	–80.39

NSD Analysis of the adsorbed octa- and tetra-halogeno TPP derivates with the Tb(III) ion indicates that all the optimized porphyrin macrocycle conformations are less puckered in comparison to the isolated structures, with domination of the dom distortion mode, as is expected from the metal ion size (Tables IV and VII). In all cases of tetrahalogeno substituted Tb(III) complexes, the metal is located exactly above the hole of the graphite hexagon, at a very small distance, which is explained by the strong attractive M–π interactions.

TABLE VII. Results of the normal-coordinate structural decomposition (NSD) analysis for the equilibrium, adsorbed metalloporphyrins conformations. D_{oop} is the total out-of-plane distortion (in Å)

Species	D_{oop}	*sad*	*ruf*	*dom*	*wav(x)*	*wav(y)*	*pro*
			Ni(II)Br$_x$TPP				
Br_8	3.7438	3.7419	0.0109	0.1210	0.0046	0.0070	0.0037
ct-Br_4	0.9487	0.6100	0.0244	0.7253	0.0212	0.0258	0.0120
tt-Br_4	1.0535	0.0218	0.8121	0.5954	0.0085	0.0072	0.3083
wm-Br_4	0.7426	0.0140	0.0250	0.6912	0.0251	0.0144	0.2683
			Ni(II)Cl$_x$TPP				
Cl_8	3.2494	3.2282	0.0127	0.3700	0.0077	0.0145	0.0035
ct-Cl_4	0.8474	0.5568	0.0264	0.6379	0.0138	0.0122	0.0152
tt-Cl_4	1.0333	0.0812	0.7823	0.6282	0.0145	0.0109	0.2326
wm-Cl_4	0.7060	0.0142	0.0331	0.6283	0.0279	0.0129	0.3186
			Tb(III)Br$_x$TPP				
Br_8	1.7730	0.4255	0.2486	1.6281	0.3444	0.2889	0.2185
ct-Br_4	1.0064	0.3849	0.0166	0.9108	0.0140	0.1859	0.0043
tt-Br_4	1.1030	0.0035	0.3914	1.0310	0.0146	0.0138	0.0067
wm-Br_4	1.0332	0.0081	0.0173	1.0159	0.0161	0.0086	0.1865
			Tb(III)Cl$_x$TPP				
Cl_8	0.9799	0.3491	0.0067	0.8116	0.4237	0.0078	0.0112
ct-Cl_4	1.1660	0.3334	0.0179	1.1171	0.0101	0.0057	0.0127
tt-Cl_4	1.2808	0.0147	0.4852	1.1894	0.0092	0.0077	0.0223
wm-Cl_4	0.7344	0.0382	0.0075	0.7097	0.0147	0.0074	0.1841

Again, the octahalogeno derivates of Tb(III) cannot approach close to the graphite surface, resulting in a similar conformation of the porphyrin core in comparison to the isolated structures.

CONCLUSIONS

The main goal of this study was the development of a new force field for metalloporphyrins using the CFF conformational program. This means that the previous force field was supplemented with a new function which describes the deviation of the atoms from planarity, i.e., an out-of-plane bending function. This function was parameterized and all other parameters were reoptimized in order to improve the consistency of the entire force field. The force field was parameterized on planar and highly puckered complexes, whereby the obtained structural results are in good agreement with the published MM results and with the available crystal structures.8–10 The very good agreement between the calculated and experimental structures is the best indicator of the successful augmentation of the new function and the valid reoptimization of the force field. With essentially the same force field, the effects of the peripheral substitution and the nature of the central metal atom as well as the influence of a presence of graphite (0001) surface on the non-planar distortions of octa- and tetrahalogeno

TPP derivates with Ni(II) and Tb(III) ions were analyzed. It was shown that both metallation and peripheral substitution determine the type and degree of non-planar deformations of porphyrin macrocycle, as a result of various strain-relieving mechanisms. An increase of the radius of the central metal atom enhances the doming of the porphyrin macrocycle, thus dom deformation is present in all of the isomers of the Tb(III) ion. Dodeca-substituted porphyrins showed a large deviation from planarity and relieved their strain predominantly by saddling of the porphyrin core, irrespective of the size of the central metal atom and the nature of the halogeno substituents. The position of the four halogeno atoms in the tetrahalogeno TPP structures has profound consequences on the mode and amount of normal distortions. In almost all cases, the wm isomer is the most stable one, except for the tetrabromo TPP Tb(III) species, when the ct isomer was found to be the most stable, but the energy difference between this and the wm isomer is small. Octahalogeno TPP derivates of Ni(II) and Tb(III) adsorbed on a graphite layer have similar conformations of porphyrin core in comparison to the isolated structures, because they cannot approach close to the graphite surface. All tetrahalogeno TPP structures are more planar in comparison to the isolated structures, as the result of π-stacking interactions. NSD analysis revealed that dom distortion is present in almost all of the structures adsorbed on a graphite layer and the origin of this distorsion can be explained by M–π interactions. If an analyzed molecule is closer to the substrate, doming is more significant. These results indicate that changes of physical and chemical properties of porphyrin adsorbed on a surface (in the present case a graphite layer) can be explained not only by the adsorption process, but also by specific conformational changes.

SUPPLEMENTARY MATERIAL

CFF parameters for metalloporphyrins are available electronically from http://www.shd.org.rs/JSCS/, or from the corresponding author on request.

Acknowledgements. This work was financially supported by the Ministry of Science and Technological Development of the Republic of Serbia.

ИЗВОД

КОНЗИСТЕНТНО ПОЉЕ СИЛА ЗА МЕТАЛОПОРФИРИНЕ

ЉУБИЦА АНЂЕЛКОВИЋ[1], СОЊА ГРУБИШИЋ[1], ИВАНА ЂОРЂЕВИЋ[1], МАТИЈА ЗЛАТАР[1], СВЕТОЗАР НИКЕТИЋ[1] и МАЈА ГРУДЕН-ПАВЛОВИЋ[2]

[1]Центар за хемију, Институт за хемију, технологију и металургију, Универзитет у Београду, Његошева 12, 11001 Београд и [2]Хемијски факултет, Универзитет у Београду, 11001 Београд

Конзистентно поље сила (CFF) за молекулско моделирање металопорфирина, које укључује новоуведену *out-of-plane* функцију, параметризовано је на основу кристалних структура Ni(II)-порфирина, никал(II)-моно-терцбутилпорфирина, никал(II)-ди-терцбутилпорфирина, никал(II)-тетрафенилпорфирина и никал(II)-октаетил-тетрафенилпорфирина. Оно је употребљено за проучавање утицаја величине централног металног јона, периферне супсти-

туције као и утицаја присутног супстрата на конформације порфиринског језгра код окта- и тетрахалогено-тетрафенилпорфирина са Ni(II) и Tb(III). Јединствене равнотежне структуре, добијене на основу молекулско-механичких прорачуна великог броја почетних структура, показују добро слагање са кристалним структурама, као и са претходно публикованим резултатима, не само у метричким подацима, већ и у начину набирања порфиринског језгра. Метод нормалне-координатне структурне декомпозиције (NSD) омогућава да се на једнозначан начин опише свака оптимизована конформација добијена молекулско-механичким прорачунима.

(Примљено 1. јула 2010)

REFERENCES

1. I. D. Kostas, A. G. Coutsolelos, G. Charalambidis, A. Skondra, *Tetrahedron Lett.* **48** (2007) 6688
2. Y. Higuchi, M. Kusunoki, N. Yasuoka, M. Kakudo, *J. Mol. Biol.* **172** (1984) 109
3. G. Fermi, M. F. Perutz, B. Shaanan, R. Fourme, *J. Mol. Biol.* **175** (1984) 159
4. B. C. Finzel, T. L. Poulos, J. Kraut, *J. Biol. Chem.* **259** (1984) 13027
5. G. V. Louie, G. D. Brayer, *J. Mol. Biol.* **214** (1990) 527
6. M. O. Senge, in *The Porphyrin Handbook*, Vol. 1, K. M. Kadish, K. M. Smith, R. Guilard, Eds., Academic Press, New York, 2000, p. 239
7. X. Song, W. Jentzen, L. Jaquinod, R. G. Khoury, C. J. Medforth, S. L. Jia, J. G. Ma, K. M. Smith, J. A. Shelnutt, *Inorg. Chem.* **37** (1998) 2117
8. M. Gruden, S. Grubišić, A. G. Coutsolelos, S. R. Niketić, *J. Mol. Struct.* **595** (2001) 209
9. M. Gruden-Pavlović, S. Grubišić, S. R. Niketić, *J. Inorg. Biochem.* **98** (2004) 1293
10. M. Gruden-Pavlović, S. Grubišić, M. Zlatar, S. R. Niketić, *Int. J. Mol. Sci.* **8** (2007) 810
11. W. Jentzen, X. Z. Song, J. A. Shelnutt, *J. Phys. Chem. B* **101** (1997) 1684
12. J. A. Shelnutt, X. Z. Song, J. G. Ma, S. L. Jia, W. Jentzen, C. J. Medforth, *Chem. Soc. Rev.* **27** (1998) 31
13. M. Zimmer, *Coord. Chem. Rev.* **253** (2009) 817
14. S. R. Niketić, K. Rasmussen, *The Consistent Force Field: A Documentation, Lecture Notes in Chemistry*, Springer, Berlin, 1977
15. K. Rasmussen, *Potential Energy Functions in Conformational Analysis, Lecture Notes in Chemistry*, Springer, Berlin, 1985
16. N. Raos, S. R. Niketić, V. Simeon, *J. Inorg. Biochem.* **16** (1982) 1
17. *Gaussian 98 Pople, Revision A.6*, Gaussian Inc., Pittsburgh, PA, 1998
18. A. K. Rappé, C. J. Casewit, *Molecular Mechanics across Chemistry*, University Science Books, South Orange, NJ, 1997, p. 37.